JACS

JOURNAL OF THE AMERICAN CHEMICAL SOCIETY

Article

Non-Interpenetrated Metal−Organic Frameworks Based on Copper(II) Paddlewheel and Oligoparaxylene-Isophthalate Linkers: Synthesis, Structure, and Gas Adsorption

Yong Yan,[†,‡,×] Michal Juríček,[§,∥,×] François-Xavier Coudert,[⊥] Nicolaas A. Vermeulen,[§] Sergio Grunder,[§] Anne Dailly,[#] William Lewis,[†] Alexander. J. Blake,[†] J. Fraser Stoddart,*[,§] and Martin Schröder*[,†,‡]

[†]School of Chemistry, University of Nottingham, University Park, Nottingham NG7 2RD, U.K.

[‡]School of Chemistry, University of Manchester, Oxford Road, Manchester M13 9PL, U.K.

[§]Center for the Chemistry of Integrated Systems, Department of Chemistry, Northwestern University, 2145 Sheridan Road, Evanston, Illinois 60208, United States

[∥]Department of Chemistry, University of Basel, St. Johanns-Ring 19, 4056 Basel, Switzerland

[⊥]Chimie ParisTech, PSL Research University, CNRS, Institut de Recherche de Chimie Paris, 75005 Paris, France

[#]Chemical and Environmental Sciences Laboratory, General Motors Corporation, Warren, Michigan 48090, United States

Ⓢ *Supporting Information*

ABSTRACT: Two metal−organic framework materials, **MFM-130** and **MFM-131** (MFM = Manchester Framework Material), have been synthesized using two oligoparaxylene (OPX) tetracarboxylate linkers containing four and five aromatic rings, respectively. Both **fof**-type non-interpenetrated networks contain Kagomé lattice layers comprising $[Cu_2(COO)_4]$ paddlewheel units and isophthalates, which are pillared by the OPX linkers. Desolvated **MFM-130**, **MFM-130a**, shows permanent porosity (BET surface area of 2173 m^2/g, pore volume of 1.0 cm^3/g), high H_2 storage capacity at 77 K (5.3 wt% at 20 bar and 2.2 wt% at 1 bar), and a higher CH_4 adsorption uptake (163 $cm^3(STP)/cm^3$ (35 bar and 298 K)) compared with its structural analogue, **NOTT-103**. **MFM-130a** also shows impressive selective adsorption of C_2H_2, C_2H_4, and C_2H_6 over CH_4 at room temperature, indicating its potential for separation of C_2 hydrocarbons from CH_4. The single-crystal structure of **MFM-131** confirms that the methyl substituents of the paraxylene units block the windows in the Kagomé lattice layer of the framework, effectively inhibiting network interpenetration in **MFM-131**. This situation is to be contrasted with that of the doubly interpenetrated oligophenylene analogue, **NOTT-104**. Calculation of the mechanical properties of these two MOFs confirms and explains the instability of **MFM-131** upon desolvation in contrast to the behavior of **MFM-130**. The incorporation of paraxylene units, therefore, provides an efficient method for preventing network interpenetration as well as accessing new functional materials with modified and selective sorption properties for gas substrates.
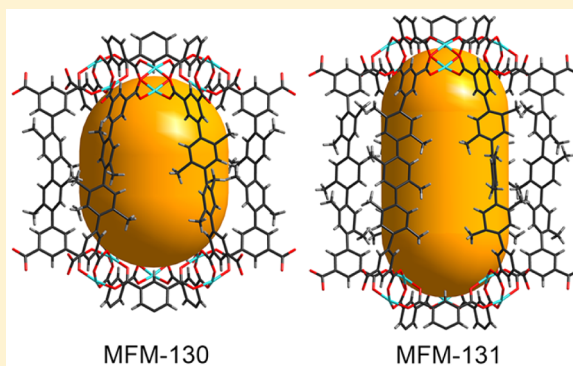
INTRODUCTION

Nanoporous metal−organic frameworks (MOFs) constructed from metal cations or clusters bridged by polyfunctional organic linkers are an important class of hybrid materials which show great promise for gas storage and separation applications.[1] An advantage of porous MOFs is that their design, structure, and properties can be varied by modification of the organic linkers, which can have different lengths, topologies, and geometries and can incorporate functional groups to enhance preferential binding of guest substrates via optimized pore shapes/diameters for molecular separation.[2] We have developed a series of framework materials employing linear tetracarboxylate linkers and $[Cu_2(COO)_4]$ paddlewheel units[3] to generate **fof**-type networks.[4] The assembly of isophthalate (benzene-3,5-dicarboxylate) units within tetracarboxylate link-

ers with $[Cu_2(COO)_4]$ paddlewheels generates two-dimensional Kagomé lattices, which are pillared by the aromatic backbones of these linkers. Two types of cage structures are formed within this assembly: Cage A, an ellipsoid-shaped cage formed by six linkers and two triangular $[(Cu_2)_3(isophthalate)_3]$ windows at the two ends, with a larger hexagonal $[(Cu_2)_6(isophthalate)_6]$ core structure, and Cage B, a more cylindrical cage formed also by six linkers and two triangular $[(Cu_2)_3(isophthalate)_3]$ windows. These materials show high porosity and high H_2 and CH_4 storage capacity, with the porosity, storage capacity, and binding energies with H_2 and CH_4 being tuned by modification of the organic linkers.[3]

Elongation of the linear tetracarboxylate units can increase the porosity of the resultant structures,[3b] but network interpenetration in these **fof**-systems can occur when the linker is lengthened beyond a certain point. Thus, development of highly porous and non-interpenetrated structures in these systems remains a challenge.[5] There are several strategies for building non-interpenetrated networks with large organic linkers: (i) building networks with intrinsically non-interpenetrating topologies, such as **rht**[6] and **flu**;[7] (ii) optimizing the synthesis of MOF materials using different solvents, conditions, and template effects to target preferred non-interpenetrating networks;[8] and (iii) introducing bulky functional groups in the organic units to create steric hindrance.[9]

Oligoparaxylenes (OPXs) have been developed as efficient building blocks for the construction of MOFs with Zn(II)/Mg(II) nodes.[10,11] The methyl substituents present in OPXs increase dramatically the solubility of longer oligomers compared to oligophenylene analogues, which become increasingly less soluble with increasing length over just a few aromatic rings. OPX linkers can thus serve as stable, extended, and, most importantly, soluble organic building units or struts. A series of non-interpenetrating **MOF-74** analogues have been successfully constructed from 4-carboxylate OPX tectons to give a series of isoreticular Mg(II) frameworks with pore apertures ranging from 1.4 to 9.8 nm.[11] We reasoned that the synthesis of non-interpenetrating **fof**-type network structures might be achieved using OPX units serving as linear aromatic backbones to connect two isophthalate units to form extended, yet soluble, tetracarboxylate linkers. We envisaged that frameworks with optimized pore size, geometry, and functionality could be accessed by employing such OPX-derived linkers rather than using the more problematic, insoluble oligophenylene units. It is worth noting that methyl substituents present in the OPX struts can not only create hydrophobic pockets,[3e] which can aid gas adsorption and separation, but can also impart a degree of steric bulk within pores.

We report herein the synthesis of two new OPX-based linkers, the tetracarboxylates H_4L^{IV} and H_4L^V (Figure 1), incorporating isophthalate moieties, and their coordination to $[Cu_2(COO)_4]$ paddlewheel nodes to form the non-interpenetrated **fof**-type frameworks **MFM-130** and **MFM-131**. **MFM-131** is the first example of a **fof**-type MOF with ultra-long organic struts that does not show network interpenetration. The adsorption of H_2, CH_4, CO_2, and small

hydrocarbons in the desolvated form of **MFM-130**, **MFM-130a**, has been investigated, and the selective adsorption of CO_2 over N_2, and C_2 hydrocarbons (acetylene, ethylene, and ethane) over CH_4 in this material is discussed. Desolvation of **MFM-131**, however, leads to collapse of this material and loss of porosity. Calculation of the mechanical properties of these two MOFs in the elastic regime was, therefore, performed to confirm and explain their distinct properties upon desolvation.

■ EXPERIMENTAL SECTION

Materials and Instrumentation. All reagents were purchased from commercial suppliers and used without further purification unless stated otherwise. 4,4′-Diiodo-2,2′,5,5′-tetramethyl-1,1′-biphenyl was synthesized as previously reported.[12] Thin-layer chromatography (TLC) was performed on Merck TLC plates (F254 indicator), and column chromatography carried out on Merck silica gel 60 (Merck grade 9385, 0.040−0.063 mm). Nuclear magnetic resonance (NMR) spectra were recorded on a BrukerAvance III 500 MHz NMR spectrometer at working frequencies of 499.842 (^{1}H) and 125.579 (^{13}C) MHz. The signal corresponding to the residual non-deuterated solvent (CDCl$_3$: δ_H = 7.26 ppm and δ_C = 77.16 ppm; DMSO-d_6: δ_H = 2.50 ppm and δ_C = 39.52 ppm; PhMe-d_8: δ_H = 2.08 ppm and δ_C = 20.43 ppm) was used as a reference. Solutions of 1 and 4 in PhMe-d_8 were preheated at 90 °C for 30 min before acquiring their ^{1}H and ^{13}C NMR spectra at 25 °C. High-resolution mass spectra (HRMS) were measured on an Agilent 6210 time-of-flight (ToF) LC-MS using an ESI source coupled with Agilent 1100 HPLC stack via direct infusion (0.6 mL/min). Fourier-transform infrared (FTIR) spectra were performed on a Nicolet iS5 spectrometer using the attenuated total reflectance (ATR) mode. Elemental analyses were carried out on a CE-440 elemental analyzer, and thermogravimetric analyses (TGA) were performed using a TA SDT-600 thermogravimetric analyzer under a flow of N$_2$ (20 mL/min) with a heating rate of 5 °C/min. Powder X-ray diffraction (PXRD) measurements were carried out at room temperature on a PANalytical X'Pert PRO diffractometer with Cu Kα_1 radiation (λ = 1.5406 Å) at 40 kV, 40 mA with a scan speed of 0.02°/s and a step size of 0.005° in 2θ (Figures S2 and S3).

Gas Sorption Measurements. H$_2$, CO$_2$, and N$_2$ isotherms were collected using an IGA gravimetric adsorption apparatus (Hiden) in a clean ultra-high-vacuum system with a diaphragm and turbo pumping system. Approximately 120 mg of solvent-exchanged sample was loaded into the sample basket within the adsorption instrument and then degassed under dynamic vacuum at 110 °C for 12 h to obtain the fully desolvated sample. In H$_2$ adsorption experiments, ultra-pure plus grade H$_2$ (99.9995%, BOC Gases) was purified further using calcium aluminosilicate and activated carbon adsorbents to remove trace amounts of water and other impurities before introduction into the IGA system. Volumetric CH$_4$ sorption measurements were performed over the pressure range 0−70 bar using an automatically controlled Sievert's apparatus (PCT-Pro 2000 from Hy-Energy LLC). Low-pressure (<1 bar) adsorption measurements for C$_2$ hydrocarbons were performed using an Autosorb 1-MP instrument (Quantachrome Instruments). Ultra-high-purity grade C$_2$H$_2$, C$_2$H$_4$, and C$_2$H$_6$ were used for adsorption measurements.

The temperature-dependent adsorption data were analyzed using the virial equation:[13]

$$\ln(n/p) = A_0 + A_1 n + A_2 n^2 + \ldots$$

where p is pressure, n is the amount adsorbed, and A_0, A_1, etc. are virial coefficients. The Henry's law constant (K_H) is equal to $\exp(A_0)$, and the selectivity can be derived from the ratio of the constants K_H for different gases.

Synthesis of H_4L^{IV}. *2′,2″,5′,5″-Tetramethyl-[1,1′:4′,1″:4″,1‴-quaterphenyl]-3,3‴,5,5‴-tetracarboxylate Tetramethyl Ester (1).* A mixture of 5-(4,4,5,5-tetramethyl-1,3,2-dioxaborolan-2-yl)benzene-1,3-dicarboxylate dimethyl ester (1.66 g, 5.17 mmol), 4,4′-diiodo-2,2′,5,5′-tetramethyl-1,1′-biphenyl (1.09 g, 2.35 mmol), PdCl$_2$(dppf)·CH$_2$Cl$_2$ (0.20 g, 0.24 mmol), CsF (2.14 g, 14.1 mmol), *p*-dioxane (10 mL),
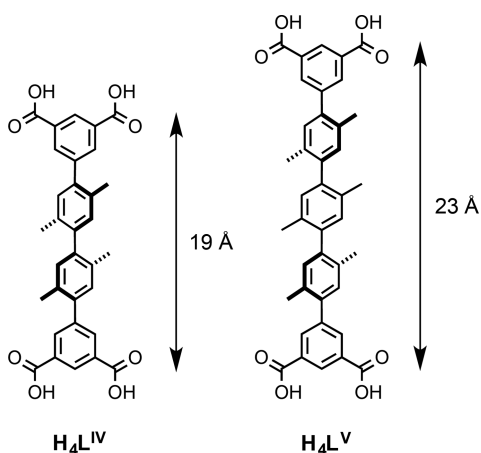

Figure 1. OPX-based tetracarboxylate linkers H_4L^{IV} and H_4L^V.

and H$_2$O (5 mL) was heated at reflux for 18 h under Ar before H$_2$O (50 mL) was added. The reaction mixture was extracted twice with CH$_2$Cl$_2$, and the combined organic extracts were washed with brine and dried over MgSO$_4$. After filtration, the solvent was removed by evaporation and the residue purified by column chromatography over silica gel using hexane/CH$_2$Cl$_2$ (1:1 to 0:1) as eluent to afford the pure product (1.16 g, 83%) as a white solid and as a mixture of two enantiomers (R and S), undergoing fast racemization at room temperature. ^{1}H NMR (500 MHz, PhMe-d_8, ppm): δ 8.94 (t, J = 1.6 Hz, 2H), 8.41 (d, J = 1.6 Hz, 4H), 7.11 (s, 2H), 7.04 (s, 2H), 3.52 (s, 12H), 2.16 (s, 6H), 2.06 (s, 6H). ^{13}C NMR (125 MHz, PhMe-d_8, ppm): δ (one signal could not be detected because of the signal overlap) 165.8, 143.1, 141.6, 139.3, 134.7, 133.9, 132.7, 131.9, 131.6, 131.3, 51.8, 19.9, 19.4. HRMS (ESI): m/z calcd for C$_{36}$H$_{34}$O$_8$: 595.2326 ([M + H]$^+$); found 595.2330.

2′,2″,5′,5″-Tetramethyl-[1,1′:4′,1″:4″,1‴-quaterphenyl]-3,3‴,5,5‴-tetracarboxylic Acid (H$_4$L^{IV}). A mixture of 1 (1.12 g, 1.88 mmol), aqueous NaOH (0.5 M, 30 mL), and THF (30 mL) was heated at 50 °C for 21 h. THF was then removed by evaporation and concentrated HCl added (pH ∼1) to the aqueous residue. The precipitate thus formed was collected by filtration, washed with H$_2$O, and dried in air to afford the product (975 mg, 97%) as a white solid and as a mixture of two enantiomers (R and S), undergoing fast racemization at room temperature. ^{1}H NMR (500 MHz, DMSO-d_6, ppm): δ 13.48 (br, 4H), 8.48 (t, J = 1.6 Hz, 2H), 8.14 (d, J = 1.5 Hz, 4H), 7.25 (s, 2H), 7.11 (s, 2H), 2.24 (s, 6H), 2.09 (s, 6H). ^{13}C NMR (125 MHz, DMSO-d_6, ppm): δ 166.6, 141.8, 140.5, 138.3, 133.7, 133.3, 131.9, 131.6, 131.4, 131.0, 128.5, 19.6, 19.1. HRMS (ESI): m/z calcd for C$_{32}$H$_{26}$O$_8$: 537.1555 ([M − H]$^−$); found 537.1544.

Synthesis of H$_4$L^V. *4′-Bromo-2′,5′-dimethyl-[1,1′-biphenyl]-3,5-dicarboxylate Dimethyl Ester (2).* A mixture of 5-(4,4,5,5-tetramethyl-1,3,2-dioxaborolan-2-yl)benzene-1,3-dicarboxylate dimethyl ester (3.56 g, 11.1 mmol), 1,4-dibromo-2,5-dimethylbenzene (14.6 g, 55.5 mmol), PdCl$_2$(dppf)·CH$_2$Cl$_2$ (0.46 g, 0.56 mmol), CsF (5.06 g, 33.3 mmol), p-dioxane (40 mL), and H$_2$O (20 mL) was heated at reflux under Ar for 18 h before H$_2$O (100 mL) was added. The reaction mixture was extracted twice with CH$_2$Cl$_2$, and the combined organic extracts were washed with brine and dried over MgSO$_4$. After filtration, the solvent was removed by evaporation and the residue purified by column chromatography over silica gel using hexane/CH$_2$Cl$_2$ (9:1 to 0:1) as eluent to afford the pure product (5.98 g, 71%) as a white solid. ^{1}H NMR (500 MHz, CDCl$_3$, ppm): δ 8.67 (t, J = 1.6 Hz, 1H), 8.16 (d, J = 1.7 Hz, 2H), 7.47 (s, 1H), 7.09 (s, 1H), 3.96 (s, 6H), 2.39 (s, 3H), 2.19 (s, 3H). ^{13}C NMR (125 MHz, CDCl$_3$, ppm): δ 166.3, 141.8, 139.0, 135.6, 134.6, 134.4, 134.1, 132.0, 130.8, 129.5, 124.6, 52.7, 22.4, 19.7. HRMS (ESI): m/z calcd for C$_{18}$H$_{17}$BrO$_4$: 377.0383 ([M + H]$^+$); found 377.0392.

2′,5′-Dimethyl-4′-(4,4,5,5-tetramethyl-1,3,2-dioxaborolan-2-yl)-[1,1′-biphenyl]-3,5-dicarboxylate Dimethyl Ester (3). A mixture of 2 (5.71 g, 15.1 mmol), bis(pinacolato)diboron (4.22 g, 16.6 mmol), PdCl$_2$(dppf)·CH$_2$Cl$_2$ (0.62 g, 0.76 mmol), KOAc (4.46 g, 45.4 mmol), and dry DMSO (60 mL) was heated at 80 °C under Ar for 24 h before H$_2$O (400 mL) was added. The precipitate thus formed was collected by filtration and washed twice with H$_2$O (∼1 L in total) before it was dissolved in CH$_2$Cl$_2$ and the organic solution dried over MgSO$_4$. After filtration, the solvent was removed by evaporation and the residue purified by column chromatography over silica gel using hexane/CH$_2$Cl$_2$ (1:1 to 0:1) as eluent to afford the pure product (5.20 g, 87%) as a white solid. ^{1}H NMR (500 MHz, CDCl$_3$, ppm): δ 8.66 (t, J = 1.7 Hz, 1H), 8.19 (d, J = 1.6 Hz, 2H), 7.69 (s, 1H), 7.05 (s, 1H), 3.96 (s, 6H), 2.54 (s, 3H), 2.22 (s, 3H), 1.37 (s, 12H). ^{13}C NMR (125 MHz, CDCl$_3$, ppm): δ (one signal could not be detected because of the signal overlap) 166.4, 142.8, 142.7, 142.1, 138.2, 134.4, 131.4, 131.2, 130.6, 129.2, 83.6, 52.6, 25.0, 21.8, 19.7. HRMS (ESI): m/z calcd for C$_{24}$H$_{29}$BO$_6$: 425.2134 ([M + H]$^+$); found 425.2140.

2′,2″,2‴,5′,5″,5‴-Hexamethyl-[1,1′:4′,1″:4″,1‴:4‴,1⁗-quinquephenyl]-3,3⁗,5,5⁗-tetracarboxylate Tetramethyl Ester (4). A mixture of 3 (1.67 g, 4.21 mmol), 1,4-diiodo-2,5-dimethylbenzene (0.726 g, 2.00 mmol), PdCl$_2$(dppf)·CH$_2$Cl$_2$ (0.16 g, 0.20 mmol), CsF (1.82 g, 12.0 mmol), p-dioxane (8 mL), and H$_2$O (4 mL) was heated at reflux

under Ar for 38 h before it was cooled to room temperature. The solid was collected by filtration and washed with H$_2$O. The solid residue was purified by column chromatography over silica gel using CH$_2$Cl$_2$, CH$_2$Cl$_2$/PhMe (2:1 to 1:1), and PhMe/ethyl acetate (99.5:0.5 to 95:5) as eluents to afford the product (759 mg, 54%) as a white solid and as a ∼1:1 mixture of two diastereoisomers, a pair of enantiomers (RR and SS) and one meso isomer (RS), undergoing fast isomerization at room temperature. ^{1}H NMR (500 MHz, PhMe-d_8, ppm): δ 8.96–8.94 (m, two partially overlapped triplets, J = 1.5 Hz, 2H), 8.42–8.41 (m, two partially overlapped doublets, J = 1.5 Hz, 4H), 7.16–7.14 (m, two partially overlapped singlets, 2H), 7.12–7.10 (m, two partially overlapped singlets, 2H), 7.06–7.03 (m, two almost resolved singlets (∼1:1 ratio), 2H), 3.51 (m, two overlapped singlets, 12H), 2.17–2.15 (m, two partially overlapped singlets, 6H), 2.15−2.12 (m, two almost resolved singlets (∼1:1 ratio), 6H), 2.10–2.06 (m, two resolved singlets (∼1:1 ratio), 6H). ^{13}C NMR (125 MHz, PhMe-d_8, ppm): δ (six signals could not be detected because of the signal overlap) 165.83, 165.82, 143.1, 142.0, 141.9, 140.83, 140.80, 139.22, 139.21, 134.8, 134.0, 133.9, 133.3, 132.7, 132.6, 132.11, 132.06, 131.6, 131.31, 131.25, 131.2, 129.5, 51.80, 51.79, 19.91, 19.90, 19.64, 19.62, 19.44, 19.42. HRMS (ESI): m/z calcd for C$_{44}$H$_{42}$O$_8$: 699.2952 ([M + H]$^+$); found 699.2959.

2′,2″,2‴,5′,5″,5‴-Hexamethyl-[1,1′:4′,1″:4″,1‴:4‴,1⁗-quinquephenyl]-3,3⁗,5,5⁗-tetracarboxylic Acid (H$_4$L^V). A mixture of 4 (735 mg, 1.05 mmol), aqueous NaOH (0.5 M, 30 mL), and THF (30 mL) was heated at 50 °C for 42 h. The THF was removed by evaporation and concentrated HCl added to the aqueous residue to pH ∼1. The precipitate thus formed was collected by filtration, washed with H$_2$O, and dried in air to afford the pure product (705 mg, 98%) as a white solid and as a ∼1:1 mixture of two diastereoisomers, a pair of enantiomers (RR and SS) and one meso isomer (RS), undergoing fast isomerization at room temperature. ^{1}H NMR (500 MHz, DMSO-d_6, ppm): δ 13.40 (m, two overlapped broad singlets, 4H), 8.51–8.46 (m, two overlapped triplets, J = 1.7 Hz, 2H), 8.17–8.12 (m, two overlapped doublets, J = 1.7 Hz, 4H), 7.27–7.06 (m, six almost resolved singlets, 6H), 2.29–2.20 (m, two overlapped singlets, 6H), 2.13–2.08 (m, two overlapped singlets, 6H), 2.08–2.03 (m, two partially resolved singlets (∼1:1 ratio), 6H). ^{13}C NMR (125 MHz, DMSO-d_6, ppm): δ (11 signals could not be detected because of the signal overlap) 166.6, 141.9, 140.82, 140.79, 139.6, 138.2, 133.7, 133.27, 133.26, 132.39, 132.38, 131.9, 131.8, 131.5, 130.9, 130.50, 130.46, 128.5, 19.54, 19.45, 19.2, 19.1, 18.9. HRMS (ESI): m/z calcd for C$_{40}$H$_{34}$O$_8$: 641.2181 ([M − H]$^−$); found 641.2177.

Synthesis of [Cu$_2$(L^{IV})(H$_2$O)$_2$]·6DMF·3H$_2$O (MFM-130). H$_4$L^{IV} (50 mg, 0.093 mmol) and Cu(NO$_3$)$_2$·2.5H$_2$O (0.17 g, 0.72 mmol) were dissolved in a mixture of N,N′-dimethylformamide (DMF, 6.0 mL) and H$_2$O (0.5 mL), and the solution was placed in a pressure tube (15 mL). Upon addition of 6 M HCl (15 μL), the tube was capped and heated at 90 °C for 16 h, and a large amount of microcrystalline product precipitated. The blue crystals were collected by filtration, washed with warm DMF, and dried in air. Yield: 58.6 mg (80% based on H$_4$L^{IV}). Selected FTIR (cm^{-1}): 3404 (br, w), 2927 (w), 1657 (vs), 1626 (s), 1588 (m), 1494 (m), 1435 (m), 1417 (m), 1367 (vs), 1308 (w), 1284 (w), 1254 (m), 1187 (w), 1149 (w), 1094 (s), 1062 (m), 923 (w), 888 (w), 778 (m), 727 (s), 701 (w), 686 (w), 660 (s), 632 (w). Anal. Calcd (%) for C$_{50}$H$_{74}$Cu$_2$N$_6$O$_{19}$: C, 50.46; H, 6.27; N, 7.06. Found (%): C, 50.38; H, 5.75; N, 7.70.

Synthesis of [Cu$_2$(L^V)(H$_2$O)$_2$]·7DMF·4H$_2$O (MFM-131). H$_4$L^V (50 mg, 0.078 mmol) and Cu(NO$_3$)$_2$·2.5H$_2$O (145 mg, 0.622 mmol) were dissolved in a mixture of DMF (7.0 mL) and H$_2$O (1.0 mL) in a pressure tube (15 mL). Upon addition of 6 M HCl (20 μL), the tube was capped and heated in an oil bath at 85 °C for 48 h to afford blue crystals. The reaction mixture was allowed to cool to room temperature, and the crystals were washed with warm DMF and dried in air. Yield: 60.9 mg, 85% based on H$_4$L^V. FTIR (cm^{-1}): 3399 (br, w), 2924 (w), 1656 (vs), 1625 (s), 1589 (m), 1489 (m), 1435 (w), 1417 (w), 1367 (vs), 1303 (w), 1254 (m), 1186 (w), 1094 (s), 1062 (m), 955 (w), 887 (m), 777 (s), 736 (m), 724 (s), 700 (w), 660 (s). Anal. Calcd (%) for C$_{61}$H$_{91}$Cu$_2$N$_7$O$_{21}$: C, 52.88; H, 6.62; N, 7.08. Found (%): C, 52.48; H, 5.88; N, 7.45.

X-ray Crystallographic Analyses. Single-crystal diffraction data for **MFM-130** were collected at 150(2) K on a Bruker SMART APEX CCD area detector using graphite-monochromated Mo Kα radiation. Data for **MFM-131** were collected using synchrotron radiation at Beamline I19 at Diamond Light Source. The details for data collection are included as part of the Crystallographic Information File (CIF) in the Supporting Information. The structures were solved by the direct method and refined by full-matrix least-squares methods on F^2 using SHELXL-2013.[14] Hydrogen atoms on the ligands were placed geometrically and refined using a riding model; the hydrogen atoms of the coordinated water molecules could not be located but are included in the formula. DFIX, SADI, and PART instructions were used to deal with the disorder of the paraxylene moieties in the structures. The SQUEEZE option of PLATON[15] was used to model the contribution of disordered guest molecules to the reflection intensities.

■ RESULTS AND DISCUSSION

Single-Crystal X-ray Structures. The tetracarboxylate ligands H_4L^{IV} and H_4L^{V} (Figure 1) were synthesized by a series of Suzuki cross-coupling reactions (Scheme 1), followed by hydrolysis of the resultant tetraesters. The synthetic procedures and characterization of the target compounds and all their precursors are provided in full detail in the Experimental Section. On the basis of the lengths of these two linear struts (approximately 19 Å for H_4L^{IV} and 23 Å for

H_4L^{V}), it was anticipated that nanosized porous structures can be assembled.

Solvothermal reactions of H_4L^{IV} and H_4L^{V} with $Cu(NO_3)_2 \cdot 2.5H_2O$ in a mixture of DMF and H_2O at 80 °C for 16 h afforded blue highly crystalline solids of $[Cu_2(L^{IV})(H_2O)_2] \cdot 6DMF \cdot 3H_2O$ (**MFM-130**) and $[Cu_2(L^{V})(H_2O)_2] \cdot 7DMF \cdot 4H_2O$ (**MFM-131**), respectively. The formulae of these two compounds were confirmed by elemental analysis, single-crystal X-ray structure determinations, and TGA (Figure S1). The phase purity of the two bulk crystalline solids was confirmed by PXRD and Le Bail analyses (Figures S2−S4). Single-crystal X-ray structure analysis revealed that both **MFM-130** and **MFM-131** crystallize in the trigonal space group $R\bar{3}$. Both rhombohedral lattices in **MFM-130** and **MFM-131** have similar a-axes due to the same type of Kagomé lattice formed by the two-connected isophthalate units with four-connected $[Cu_2(COO)_4]$ paddlewheels. In **MFM-130** (Figure 2), because of the steric hindrance caused by methyl substituents, the two-connected paraxylene units in $(L^{IV})^{4-}$ are almost perpendicular to each other. The methyl group of the paraxylene unit adjacent to the isophthalate ring forces these two rings to be non-coplanar with a torsion angle of approximately 51°. Thus, the geometrical conformation of the central pair of paraxylene units lock the two terminal isophthalate moieties within the same plane, making the linker $(L^{IV})^{4-}$ a planar four-connected node when bound to $[Cu_2(COO)_4]$ paddlewheels. **MFM-130** has an **fof**-type network topology constructed by the packing of two types of cages (A and B), and is isostructural with the analogous **NOTT-102** constructed from tetracarboxylate linkers containing phenylene instead of paraxylene units.[3b] With the methyl groups projecting into the pores, both Cage A and Cage B in **MFM-130** have reduced accessible voids compared to those of the non-functionalized analogue **NOTT-102**. Cage A has a slim ellipsoid shape with a length of 33 Å, a narrow diameter of 7 Å at the two ends and a larger diameter of 18 Å in the center, while Cage B has a thicker cylindrical shape with diameter of 13 Å and length of 16 Å (Figure 2).

MFM-131 has the same **fof** topology as **MFM-130** with the Kagomé nets pillared by three consecutive paraxylene units from $(L^{V})^{4-}$ (Figure 3). Significantly, **MFM-131** is non-interpenetrating despite the extra-long strut $(L^{V})^{4-}$ used, and this is a rare example of a **fof** framework with large internal voids (63%). Cage A in **MFM-131** is significantly elongated to 42 Å in length compared to **MFM-130** (33 Å) due to the presence of an additional paraxylene unit in the tetracarboxylate strut. With a dense population of methyl groups on the walls of the cage, the diameters of the two ends of the ellipsoid are narrowed to 5 Å compared to the oligophenylene analogue **NOTT-104**. Cage B in **MFM-131** is an elongated nanosized cylinder of 13 Å × 20 Å (13 Å × 16 Å for **MFM-130**). The structural analogue **NOTT-104**[3b] constructed from a linear tetracarboxylate linker incorporates the same length of strut used in **MFM-131**, but without the methyl groups. In this case, two identical **fof**-type lattices interpenetrate to form a doubly interpenetrated network in **NOTT-104** (Figure 3c). The $[Cu(isophthalate)]_n$ Kagomé lattice in **NOTT-104** has two types of windows: a smaller triangular window $[(Cu_2)_3(isophthalate)_3]$ of 6 Å in diameter and a larger hexagonal window $[(Cu_2)_6(isophthalate)_6]$ with an opening of 18 Å. Therefore, the narrow end of the ellipsoidal cage from one framework can cross through the wider central opening of a second network, thus allowing network interpenetration in **NOTT-104**. The $\pi-\pi$ interaction between the phenylene units from two

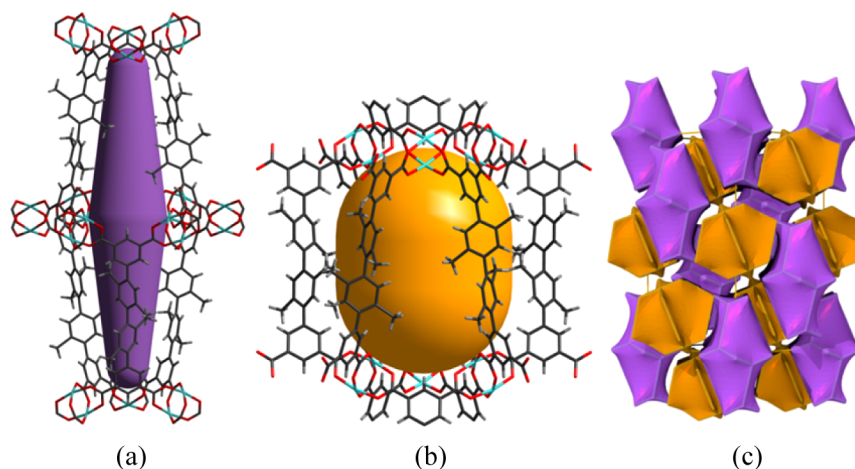## Scheme 1. Synthesis of H_4L^{IV} and H_4L^{V}
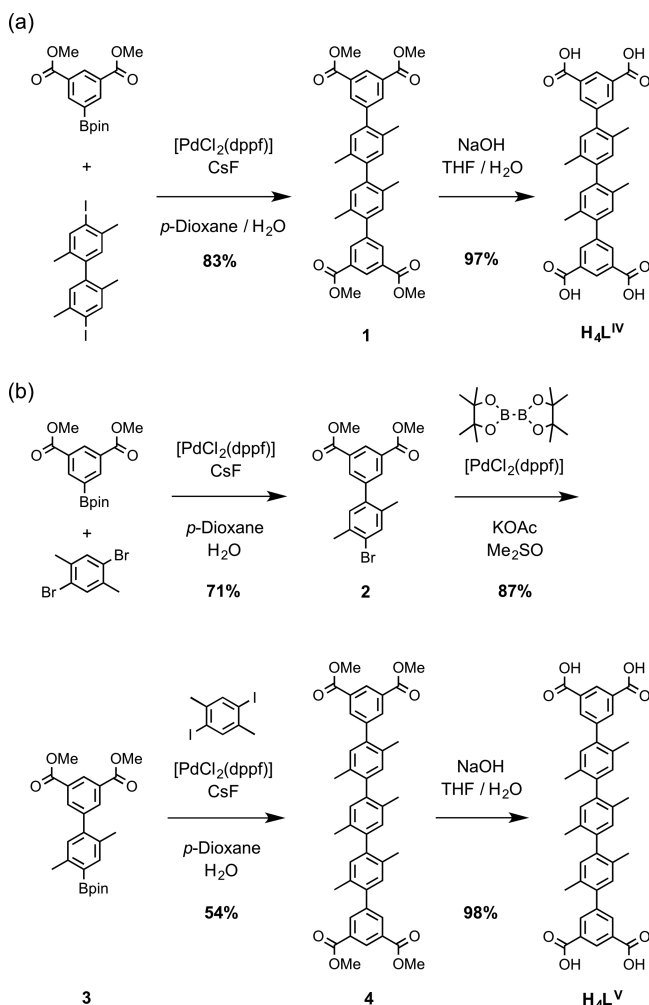
Figure 2. Views of the single-crystal X-ray structure of **MFM-130** comprising two types of cages: (a) an ellipsoid-shaped cage A of length 33 Å, comprising six $(L^{IV})^{4-}$ units and 12 $[Cu_2(COO)_4]$ paddlewheels, and (b) a cylindrical cage B (13 Å × 16 Å), formed by 12 linkers and six $[Cu_2(COO)_4]$ paddlewheels. (c) View of **fof**-type network and the natural tiling of the two types of cages in the framework.
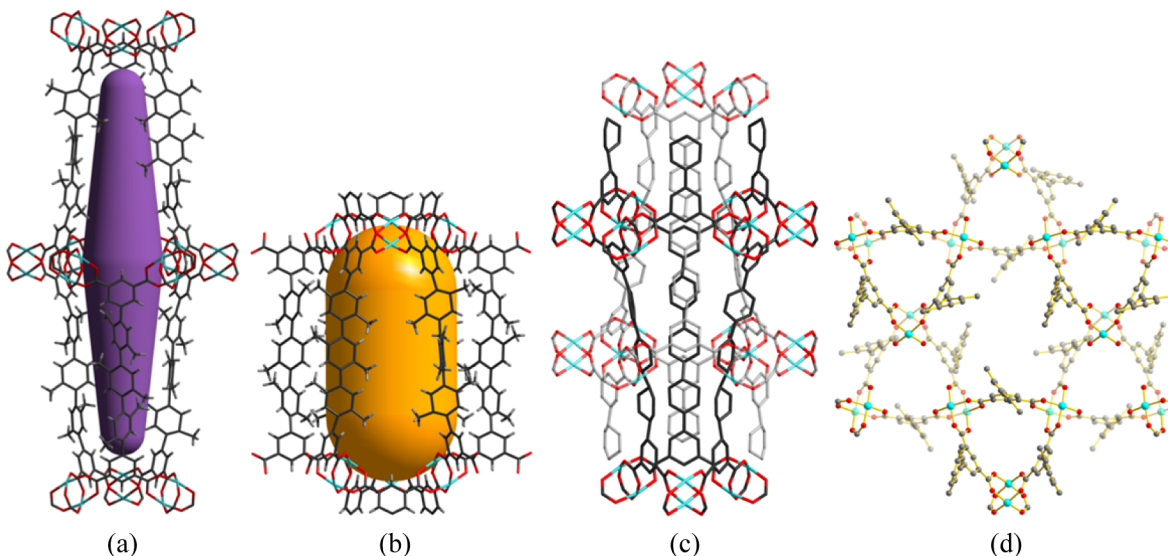

Figure 3. Views of the single-crystal X-ray structure of non-interpenetrated **MFM-131**: (a) Cage A, 42 Å in length, and (b) Cage B, with dimensions of 13 Å × 20 Å. (c) View of the interpenetrating network in **NOTT-104**. (d) View of the triangular window in the Kagomé lattice in the **MFM-131** framework. The paraxylene rings adjacent to the triangular windows block the space and do not allow the two independent networks to interpenetrate.

different networks further facilitates and stabilizes the network interpenetration. In **MFM-131**, the opening of the hexagonal window in the Kagomé lattice is significantly smaller because of the presence of six paraxylene units around the window and π−π interactions between the paraxylene units are inhibited, thus successfully preventing interpenetration of the two **fof** lattices.

Stabilities of MFM-130 and MFM-131 and Mechanical Property Calculations. The activation of as-synthesized **MFM-130** and **MFM-131** was investigated for subsequent gas adsorption studies. Both materials were exchanged with acetone for 24 h before being dried under vacuum at 110 °C to afford the desolvated samples **MFM-130a** and **MFM-131a**, respectively. **MFM-130a** maintained crystallinity after thermal treatment under vacuum as confirmed by the PXRD analysis (Figure S2). However, after the desolvation process (using both thermal treatment and supercritical CO_2 drying) **MFM-131** showed almost complete loss of crystallinity, indicating an

inherent instability upon desolvation. In order to understand and rationalize the reasons behind the distinct behaviors of **MFM-130** and **MFM-131** upon desolvation, we calculated the mechanical properties of both structures in the elastic regime (see Supporting Information).[16,17] The second-order elastic stiffness tensors are shown in Figures S7 and S8, and a summary of their average and directional elastic properties is presented in Table 1. It can be observed that both structures have relatively similar mechanical features (due to their isostructural nature), including a marked anisotropy with stiffer directions (as defined by high Young's modulus) along or near the c axis which is, on average, the principal axis of the organic linkers. Surprisingly, both structures display remarkable negative linear compressibility along the c axis (−59.9 TPa^{-1} for **MFM-130** and −67.6 TPa^{-1} for **MFM-131**), which we attribute to a hinging mechanism in the **fof** topology.[18] This suggests that testing of **MFM-130**, **MFM-131**, and other MOFs

Table 1. Summary of the Mechanical Properties of the Structural Models of MFM-130 and MFM-131 in the Elastic Regime

elastic property	MFM-130	MFM-131
bulk modulus (Hill average) (GPa)	11.41	8.77
Young's modulus (Hill average) (GPa)	7.79	4.69
shear modulus (Hill average) (GPa)	2.81	1.66
minimal Young's modulus (GPa)	4.43	1.42
maximal Young's modulus (GPa)	11.25	12.84
minimal shear modulus (GPa)	1.73	0.48
maximal shear modulus (GPa)	4.25	2.52
largest negative linear compressibility (TPa^{-1})	−59.9	−67.6
largest positive linear compressibility (TPa^{-1})	96.7	136.9

of **fof** topology under pressure may generate unusual dynamic effects.

The main difference in the mechanical properties of **MFM-130** and **MFM-131** turns out to be the value of their lowest elastic modulus: the shear modulus (Figure 4). While **MFM-131** shows lower average Young's and shear moduli than **MFM-130**, **MFM-131** shows an especially low directional shear modulus of 0.48 GPa compared to 1.73 GPa for **MFM-130**. This difference is linked to the lower density and higher porosity of **MFM-131** and not to any change in mechanism since both minimal shear moduli correspond to the same direction. The very low shear modulus of **MFM-131** is, to our knowledge, the lowest ever calculated for a non-flexible MOF. It explains the low resistance of **MFM-131** to solvent

evacuation, during which shear forces develop inside the crystal and which can, if they exceed the shear modulus in a specific direction, lead to mechanical instability and trigger a structural transition or collapse. This behavior is similar to the instability shown by some experimentally synthesized ZIF structures upon removal of solvents and guest molecules,[19] suggesting that a gentler method of desolvation needs to be developed for the highly porous **MFM-131** to remain structurally intact upon activation. However, with its densely functionalized methyl groups and large pore structure, **MFM-131** may find other applications such as sensing and catalysis where desolvation is not required for the process. The above calculation represents a unique example of how computational simulation of the mechanical properties of MOFs, in this case, a **fof**-type system consisting of layered Kagomé lattices pillared by OPX units of different lengths, can help rationalize and explain the experimental results. This also improves our understanding of the mechanochemical properties of MOFs, especially those with large pore structures comprising large organic units.

Porosity of MFM-130a. The total accessible volume in **MFM-130a** after removal of guest solvates and coordinated water molecules is 60% as determined by the PLATON/VOID routine,[15] and the desolvated framework has a calculated density of 0.642 g/cm^3, which is more dense than **NOTT-102a** (0.587 g/cm^3) reflecting the presence of methyl functionalities in the former. The N_2 isotherm for **MFM-130a** at 77 K shows typical Type I characteristics, indicative of the microporous nature of **MFM-130a** (Figure 5). The BET surface area is 2173
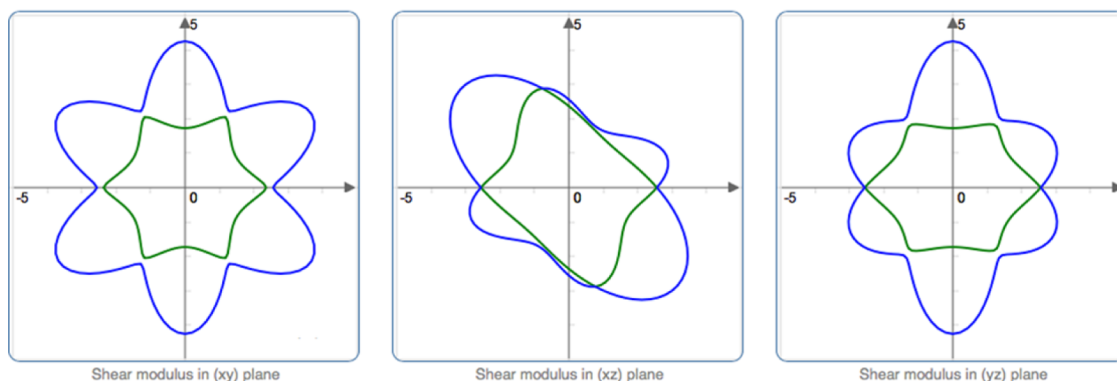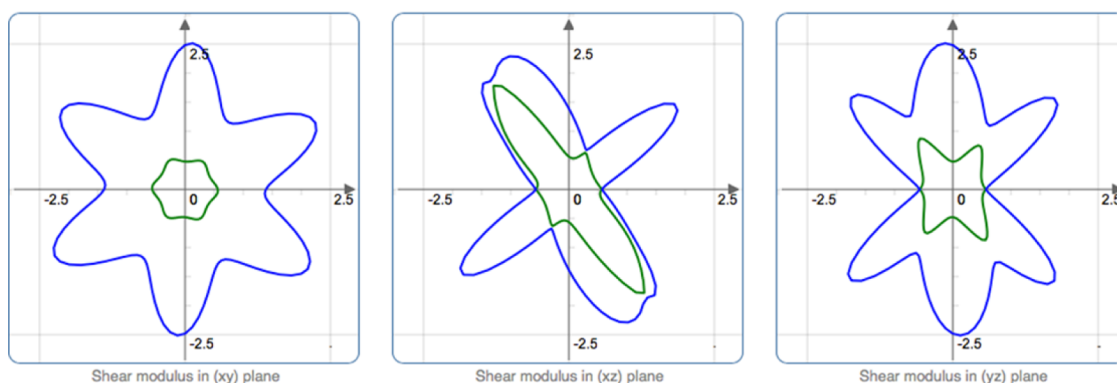

Figure 4. Directional shear modulus of **MFM-130** and **MFM-131** in the (*xy*), (*xz*), and (*yz*) planes. Minimal and maximal values of shear modulus for each direction are plotted in green and blue, respectively.
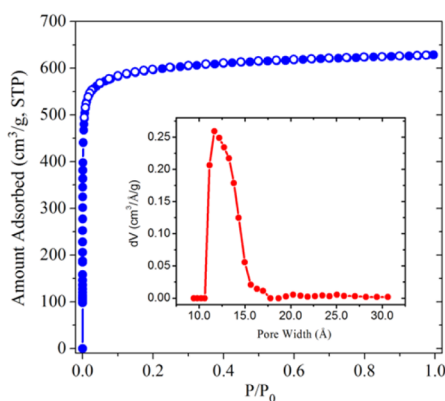
Figure 5. N_2 isotherm for **MFM-130a** at 77 K. The inset shows the pore size distribution, indicating that the pore diameters are distributed between 11 and 15 Å according to the NLDFT model.

m^2/g and total pore volume is 1.0 cm^3/g derived from the N_2 isotherm. Due to the multiple methyl substituents occupying additional space, **MFM-130a** shows both a lower BET surface area and total pore volume than the isostructural frameworks **NOTT-102**,[3b] **NOTT-110**,[3c] and **NOTT-111**[3c] containing biphenyl, phenanthrene, and hydrophenanthrene subunits, respectively, in the backbones of the tetracarboxylate linkers. The pore diameters in **MFM-130a** based on the nonlocal density functional theory (NLDFT) model are narrowly distributed between 11 and 15 Å.

H_2, CH_4, and CO_2 Sorption Properties of MFM-130a. Cu(II)-based MOFs have been intensively investigated for their H_2 storage properties because of their high surface area and the availability of open Cu(II) sites for providing strong H_2 binding sites.[20,21] Gravimetric H_2 sorption isotherms for **MFM-130a** were collected at 77 and 88 K up to 20 bar (Figure 6). **MFM-130a** has a lower surface area compared to non-functionalized **NOTT-102** leading to a lower H_2 adsorption capacity of 5.3 wt% at 20 bar and 77 K (6.07 wt% for **NOTT-102**), consistent with the physical sorption nature of these materials. **MFM-130a** can adsorb 2.2 wt% of H_2 at 77 K and 1 bar, higher than most other MOFs without open metal sites.[1e,22] The isosteric heat of adsorption for H_2 in **MFM-130a** was calculated to be 6.6 kJ/mol at zero coverage using the virial method, higher than those for **NOTT-102a**, **NOTT-110a** and **NOTT-111a**, confirming that the methyl groups in **MFM-130a** can increase the overlapping potential for H_2 molecules.

CH_4 storage has been widely studied due to the importance of natural gas as a promising alternative to petroleum-based fuels for mobile applications.[23] The CH_4 adsorption isotherms for **MFM-130a** have been measured at 298 and 273 K up to 20 bar using the same gravimetric method as for the H_2 measurements (Figure S6). **MFM-130a** can adsorb a total of 6.9 mmol/g (154 cm^3 (STP)/g) of CH_4 at 298 K and 20 bar, which is moderate compared to other Cu(II)-based MOF materials with high CH_4 capacities (Table 2).[23] At 273 K, the total CH_4 adsorption capacity reaches 9.0 mmol/g (203 cm^3 (STP)/g) at 20 bar. High-pressure CH_4 adsorption data up to 65 bar at 298 K were also collected using a volumetric method and the results match well with the gravimetric measurements in the range of 0−20 bar (Figure 7). The excess CH_4 uptake increases with pressure and then reaches a maximum value of 222 cm^3 (STP)/g (equivalent to 143 cm^3 (STP)/cm^3) at 47 bar. The total CH_4 uptake, calculated using the crystal and skeletal densities of the material, reaches a value of 274 cm^3
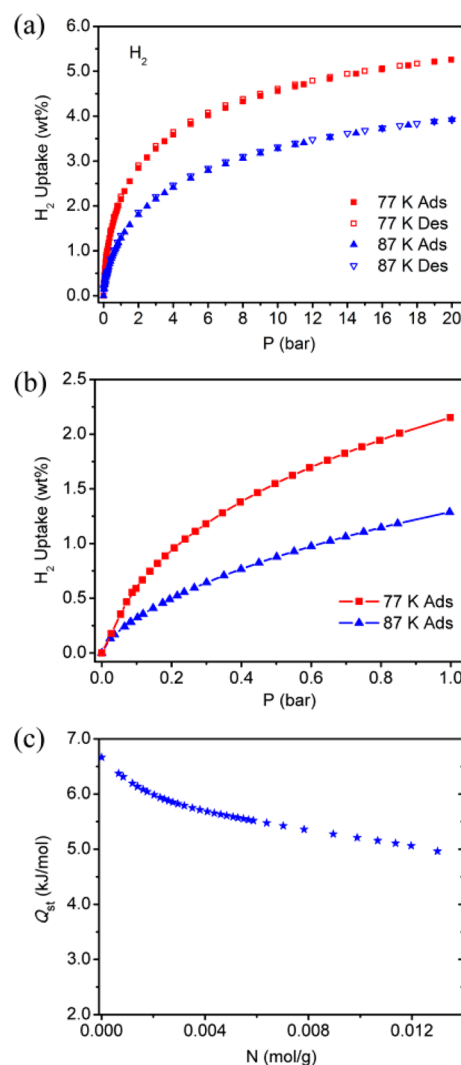

Figure 6. H_2 isotherms for **MFM-130a** at 77 and 87 K (a) up to 20 bar and (b) up to 1 bar. (c) Isosteric heat of H_2 adsorption as a function of loading for **MFM-130a**. "Ads" and "Des" represent adsorption and desorption, respectively.

(STP)/g at 65 bar, corresponding to volumetric uptake of 176 cm^3 (STP)/cm^3. At 35 bar and 298 K, although **MFM-130a** shows lower gravimetric CH_4 uptake (excess: 219 cm^3 (STP)/g; total: 254 cm^3 (STP)/g) than highly porous MOFs such as **NOTT-119**[6e] and **NU-111**,[24] it exhibits higher volumetric CH_4 capacity (excess: 141 cm^3 (STP)/cm^3; total: 163 cm^3 (STP)/cm^3, Table 2). The deliverable CH_4 capacity is also an important factor when considering a material for practical on-board CH_4 storage applications. The deliverable amount of CH_4 in **MFM-130a**, defined as the difference in uptake between 65 and 5 bar, is 131 cm^3/cm^3. To gain further insight into the nature of framework−CH_4 interactions, the isosteric heats of adsorption (Q_{st}) were calculated from isotherms collected at different temperatures. The Q_{st} for CH_4 is 16.0 kJ/mol at zero surface coverage and, importantly, remains almost constant with increased loading. At loadings higher than 5.0 mmol/g, Q_{st} starts to increase slowly due to the CH_4−CH_4 interactions, which may play an important role at high loadings.

The CO_2 and N_2 adsorption isotherms for **MFM-130a** were also measured in the pressure range of 0−1 bar at 298 and 273 K (Figure 8). The CO_2 adsorption capacities for **MFM-130a** at

Table 2. Comparisons of CH$_4$ Adsorption Data for a Variety of MOFs at 298 K

material	BET surface area (m²/g)[a]	pore volume (cm³/g)[a]	crystal density (g/cm³)	total CH₄ uptake at 20 bar		uptake at 35 bar				total CH₄ uptake at 65 bar		deliverable CH₄ amount (65 to 5 bar)	
						excess		total					
				cm³(STP)/g	v/v	cm³(STP)/g	v/v	cm³(STP)/g	v/v	cm³(STP)/g	v/v	cm³(STP)/g	v/v
MFM-130a	2173	1.0	0.642	154	99	219	141	254	163	274	176	204	131
HKUST-1[23a]	1850	0.78	0.883	207	183	231	204	257	227	300	264	215	190
NOTT-100a[23b]	1661	0.68	0.927	181	168	187	173	210	195	249	231	149	138
NOTT-101a[23b]	2805	1.08	0.684	217	148	250	171	284	194	349	239	265	181
NOTT-102a[23b]	3342	1.27	0.587	220	129	266	156	308	181	403	237	324	190
UTSA-76a[3d]	2820	1.09	0.699	234	164	263	184	302	211	367	257	281	196
NOTT-122a[6f]	3286	1.41	0.589	225	133	268[b]	155[b]	314[b]	182[b]	401[b]	232[b]	317[b]	183[b]
NOTT-119a[6e]	4118	2.35	0.361	196	71	215	78	296	107	423	153	370	134
NU-111[23a]	4930	2.09	0.409	220	90	267	109	337	138	504	206	437	179

[a]Measured by N$_2$ isotherms at 77 K. [b]These data were taken from ref 23a.
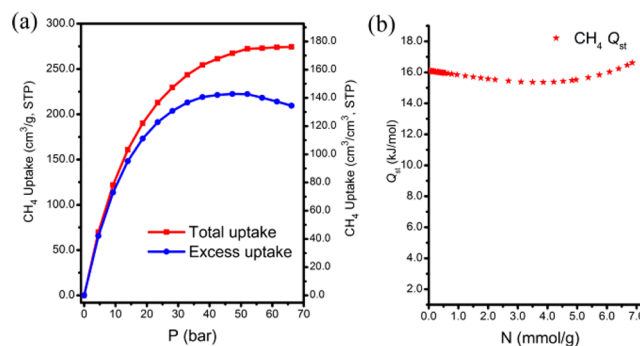
Figure 7. (a) CH$_4$ sorption in **MFM-130a** in the pressure range of 0−70 bar. (b) Variation of heat of adsorption for CH$_4$ in **MFM-130a** as a function of loading.
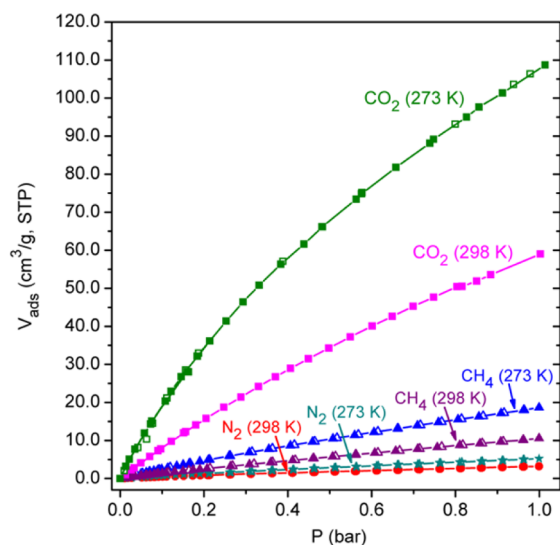
Figure 8. CO$_2$, CH$_4$, and N$_2$ adsorption isotherms for **MFM-130a** at 298 and 273 K up to 1 bar.

1 bar are 109 cm^3/g (21.3 wt%) and 59 cm^3/g (11.6 wt%) at 273 and 298 K, respectively. Although these values are lower than those for other highly porous Cu(II)-based MOF materials such as **NOTT-122**[6f] (39.7 wt% at 273 K; 20.4 wt % at 298 K) and **NOTT-125**[25] (40.0 wt% at 273 K; 18.2 wt% at 298 K), which is attributed to the smaller pore size and the absence of CO$_2$-favorable organic functionalities in **MFM-130a**, they are higher than for most other frameworks without open metal sites such as ZIFs under the same conditions.[26] The heats of adsorption for CO$_2$ were calculated based on the isotherms at different temperatures by using the virial method. **MFM-130a** shows a high heat of CO$_2$ adsorption of 26 kJ/mol at zero surface coverage, reflecting a strong framework−CO$_2$ inter-action due to the synergistic effects from the narrowed pores caused by the presence of methyl groups and open Cu(II) sites. Compared to the CO$_2$ adsorption, **MFM-130a** shows limited N$_2$ and CH$_4$ uptakes at 1 bar and room temperature. The CO$_2$/N$_2$ adsorption selectivity values for **MFM-130a** are 29.2:1 at 298 K and 38.2:1 at 273 K, as determined by evaluating the ratios of Henry's law constants from single-component isotherms. The CO$_2$/N$_2$ selectivity for **MFM-130a** is significantly higher than those for **NOTT-122a** (14.3:1) and **NOTT-125a** (16:1) at 298 K. This increase in the selective adsorption of CO$_2$ is because the methyl groups from the paraxylene units in **MFM-130a** reduce the accessible pore

volume, thus creating enhanced overlapping potential for CO_2 molecules, but at the same time, lowering the adsorption of N_2. Also, **MFM-130a** shows respectable CO_2/CH_4 selectivities of 9.4 at 273 K and 7.1 at 298 K.

Hydrocarbon Adsorption and Selectivities in MFM-130a. Light hydrocarbons (C_1-C_3) are important raw chemicals for various industrial applications, and the separation of the pure components from mixtures involves energy-intensive cryogenic distillation processes.[27] In particular, separation of C_2 hydrocarbons from CH_4 is an important industrial process for purification of CH_4, and adsorptive separation has been shown to be an efficient and energy-economic approach to these separation tasks.[28] Several MOFs have been realized for their potential excellent selectivities of C_2 hydrocarbons over CH_4 due to the fine control of pore size/shape and the presence of strong C_2 hydrocarbon binding sites in the MOF structures.[29] Although MOFs with pore sizes comparable to the kinetic diameters (3.3−4.4 Å) of C_2 hydrocarbons show enhanced C_2/C_1 selectivities,[29b,c] they typically suffer from low separation capacities. Therefore, the ideal MOFs for such separations should be ones showing optimized pore sizes and moderately high porosity, and at the same time, high affinities to C_2 hydrocarbons. Accordingly, pure-component C_2H_2, C_2H_4 and C_2H_6 isotherms for **MFM-130a** were collected at ambient temperatures (Figure 9). **MFM-130a** shows moderately high C_2H_2 uptakes of 144 cm³ (STP)/g at 273 K and 85.9 cm³/g at 298 K and 1 bar. The C_2H_2 capacities of **MFM-130a** are comparable to those of other MOFs with open metal sites showing high C_2H_2 uptakes under the same conditions (Table 3). **MFM-130a** also adsorbs high amounts of C_2H_4 (115.2 cm³/g at 273 K; 78.7 cm³/g at 298 K) and C_2H_6 (124.6 cm³/g at 273 K; 77.1 cm³/g at 298 K) at 1 bar. Compared to C_2H_2, C_2H_4, and C_2H_6, **MFM-130a** shows considerably low CH_4 uptake (18.6 cm³/g at 273 K; 10.6 cm³/g at 298 K) at 1 bar, indicating its potential for efficient separation of C_2 hydrocarbons from CH_4.

Virial analyses on the temperature-dependent hydrocarbons adsorption isotherms were performed to evaluate the binding interactions of C_2 hydrocarbons with the framework of **MFM-130a** and the separation selectivities (Table S2). The isosteric heats of adsorption at zero coverage, calculated based on the virial parameters, are 33.1, 34.0, and 25.0 kJ/mol for C_2H_2, C_2H_4, and C_2H_6, respectively (i.e., 16 kJ/mol for CH_4). It is worth noting that the C_2H_2 adsorption enthalpy for **MFM-130a** at low loading is higher than those for other Cu(II)-based MOFs such as **MOF-505** (25.4 kJ/mol) and $Cu_3(BTC)_2$ (30.4 kJ/mol),[31a] indicating that the open Cu(II) sites, coupled with the optimized pore diameter induced by the functionalization of methyl groups in **MFM-130a**, play an important role in enhancing the binding energy between C_2H_2 and the framework. The selectivities for C_2 hydrocarbons/CH_4 were derived using Henry's law constants for individual hydrocarbons, based on the equation $S_{ij} = K_H(i)/K_H(CH_4)$. **MFM-130a** reveals moderate selectivities for C_2H_6 vs CH_4 of 14.4 at 273 K and 10.1 at 298 K. This is consistent with the fact that the interactions of saturated C_2H_6 with the framework is solely based on van der Waals interactions and the selective adsorption of C_2H_6 over CH_4 is mainly based on the size effect of the adsorbates. Importantly, **MFM-130a** shows high selectivities for C_2H_2/C_2H_4 over CH_4 of 66.5/60.0 at 273 K and 34.7/30.3 at 298 K, respectively. Thus, **MFM-130a** represents a rare example of a framework material showing simultaneously high C_2 hydrocarbons adsorption capacities and high C_2 hydrocarbons/CH_4 selectivities at ambient temperature.

CONCLUSIONS

In summary, we have successfully synthesized in a novel and efficient manner two linear tetracarboxylate linkers containing paraxylene units and the respective $[Cu_2(COO)_4]$-based **fof**-type networks **MFM-130** and **MFM-131**. Both these frameworks are non-interpenetrating, despite the extra-long organic linkers used, and comprise Kagomé lattice layers pillared by the organic oligoparaxylene backbones. In these structures, the paraxylene moieties adjacent to the isothphalate units significantly reduce the accessible openings of windows in the Kagomé lattice layers, thus effectively preventing interpenetration by two networks. This study provides a novel and efficient way for generating non-interpenetrating structures by using paraxylene units as building blocks for organic struts. The mechanical properties calculated for these two MOFs revealed that **MFM-131** shows lower average Young's and shear moduli than **MFM-130**, explaining its instability upon desolvation. This approach gives further understanding of the mechanochemical properties in MOFs, especially those with large pore structures containing large organic units. The desolvated framework **MFM-130a**, densely decorated with methyl groups, shows moderately high porosity with BET surface area of 2173 m²/g and pore volume of 1.0 cm³/g, with high H_2 uptake capacities at both low and high pressures (2.2 wt% at 1 bar; 5.3 wt% at 20 bar), albeit at low temperature (77 K). The observed increased isosteric heat of adsorption for H_2 in **MFM-130a** compared to those of its structural analogues **NOTT-102a**, **NOTT-110a**,
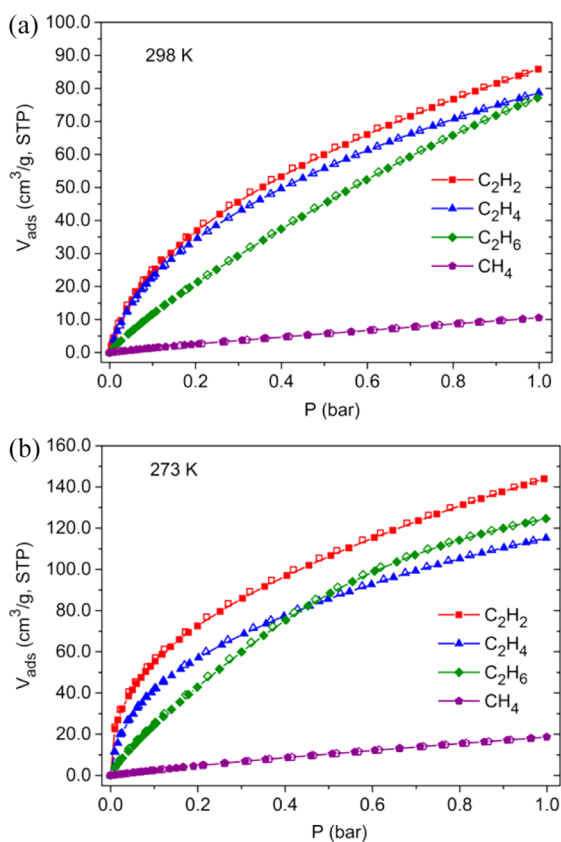

Figure 9. Adsorption isotherms for hydrocarbons in **MFM-130a** at (a) 298 and (b) 273 K in the pressure range of 0−1 bar.

Table 3. Adsorption of C_2H_2, C_2H_4, and C_2H_6 in Various MOFs at 298 K and 1 bar

material	BET surface area (m^2/g)	pore volume[a] (cm^3/g)	D_c[b] (g/cm^3)	C_2H_2 uptake (cm^3(STP)/g)	Q_{st} for C_2H_2 (kJ/mol)	C_2H_4 uptake (cm^3(STP)/g)	C_2H_6 uptake (cm^3(STP)/g)
MFM-130a	2173	1.0	0.642	85.9	33.1	78.7	77.1
Cu_2(pzdc)$_2$(pyz)[c,30]	571		1.745	42	42.5		
HKUST-1[31a]	1401	0.76	0.879	201	30.4	165.9[d]	137.7[d]
MOF-505[31a]	1139	0.68	0.927	148	25.4	113.4[d]	123.1[d]
NOTT-102a[31b]	3342	1.28	0.587	146		128.2	125.9
ZIF-8[31a]	1112		0.924	25	13.3	26.7[e]	44.2[e]
ZnMOF-74[32]	747		1.231	122	24.0		

[a]The pore volume values were calculated from N_2 isotherms at 77 K. [b]Crystal density calculated from the single-crystal structure for the activated sample. [c]pzdc = pyrazine-2,3-dicarboxylate, pyz = pyrazine. [d]These data were taken from ref 31b. [e]Measured at 301 K.[33]

and **NOTT-111a** clearly indicates that the methyl functionality can enhance the H_2−framework interactions. **MFM-130a** also shows high volumetric CH_4 adsorption (total 163 cm^3 (STP)/ cm^3 at 35 bar) and deliverable (131 cm^3/cm^3 from 65 to 5 bar) capacities at room temperature. Furthermore, the high CO_2 vs N_2, C_2H_2 vs CH_4, and C_2H_4 vs CH_4 selectivities revealed by **MFM-130a** suggest it to be a promising material for potential carbon capture and natural gas purification applications.

ASSOCIATED CONTENT

Supporting Information

The Supporting Information is available free of charge on the ACS Publications website at DOI: 10.1021/jacs.5b12312.

> TGA, PXRD analyses, gas adsorption isotherms and virial fitting parameters, and theoretical calculations, including Figures S1−S8 and Tables S1 and S2 (PDF)
> Crystallographic data for **MFM-130** and **MFM-131** (CIF)

AUTHOR INFORMATION

Corresponding Authors
*m.schroder@manchester.ac.uk
*stoddart@northwestern.edu

Author Contributions
[X]Y.Y. and M.J. contributed equally to this work.

Notes
The authors declare no competing financial interest.

ACKNOWLEDGMENTS

REFERENCES

(1) (a) Lin, X.; Jia, J.; Hubberstey, P.; Schröder, M.; Champness, N. R. CrystEngComm 2007, 9, 438−448. (b) Dincă, M.; Long, J. R. Angew. Chem., Int. Ed. 2008, 47, 6766−6779. (c) Murray, L. J.; Dincă, M.; Long, J. R. Chem. Soc. Rev. 2009, 38, 1294−1314. (d) Lin, X.; Champness, N. R.; Schröder, M. Top. Curr. Chem. 2009, 293, 35−76. (e) Suh, M. P.; Park, H. J.; Prasad, T. K.; Lim, D.-W. Chem. Rev. 2012, 112, 782−835. (f) Sumida, K.; Rogow, D. L.; Mason, J. A.; McDonald, T. M.; Bloch, E. D.; Herm, Z. R.; Bae, T.-H.; Long, J. R. Chem. Rev. 2012, 112, 724−781. (g) He, Y.; Zhou, W.; Qian, G.; Chen, B. Chem. Soc. Rev. 2014, 43, 5657−5678.

(2) (a) Zhao, D.; Timmons, D. J.; Yuan, D.; Zhou, H.-C. Acc. Chem. Res. 2011, 44, 123−133. (b) Lu, W.; Wei, Z.; Gu, Z.-Y.; Liu, T.-F.; Park, J.; Park, J.; Tian, J.; Zhang, M.; Zhang, Q.; Gentle, T., III; Bosch, M.; Zhou, H.-C. Chem. Soc. Rev. 2014, 43, 5561−5593.

(3) (a) Lin, X.; Jia, J.; Zhao, X. B.; Thomas, K. M.; Blake, A. J.; Champness, N. R.; Hubberstey, P.; Schröder, M. Angew. Chem., Int. Ed. 2006, 45, 7358−7364. (b) Lin, X.; Telepeni, I.; Blake, A. J.; Dailly, A.; Brown, C. M.; Simmons, J. M.; Zoppi, M.; Walker, G. S.; Thomas, K. T.; Mays, T. J.; Hubberstey, P.; Champness, N. R.; Schröder, M. J. Am. Chem. Soc. 2009, 131, 2159−2171. (c) Yang, S.; Lin, X.; Dailly, A.; Blake, A. J.; Champness, N. R.; Hubberstey, P.; Schröder, M. Chem. - Eur. J. 2009, 15, 4829−4835. (d) Li, B.; Wen, H.-M.; Wang, H.; Wu, H.; Tyagi, M.; Yildirim, T.; Zhou, W.; Chen, B. J. Am. Chem. Soc. 2014, 136, 6207−6210. (e) Kennedy, R. D.; Krungleviciute, V.; Clingerman, D. J.; Mondloch, J. E.; Peng, Y.; Wilmer, C. E.; Sarjeant, A. A.; Snurr, R. Q.; Hupp, J. T.; Yildirim, T.; Farha, O. K.; Mirkin, C. A. Chem. Mater. 2013, 25, 3539−3543. (f) Wang, X.-S.; Ma, S.; Rauch, K.; Simmons, J. M.; Yuan, D.; Wang, X.; Yildirim, T.; Cole, W. C.; López, J. J.; de Meijere, A.; Zhou, H.-C. Chem. Mater. 2008, 20, 3145−3152.

(4) O'Keeffe, M.; Yaghi, O. M. Chem. Rev. 2012, 112, 675−702.

(5) (a) Furukawa, H.; Ko, N.; Go, Y. B.; Aratani, N.; Choi, S. B.; Choi, E.; Yazaydin, A. O.; Snurr, R. Q.; O'Keeffe, M.; Kim, J.; Yaghi, O. M. Science 2010, 329, 424−428. (b) Farha, O. K.; Eryazici, I.; Jeong, N. C.; Hauser, B. G.; Wilmer, C. E.; Sarjeant, A. A.; Snurr, R. Q.; Nguyen, S. B. T.; Yazaydin, A. Ö.; Hupp, J. T. J. Am. Chem. Soc. 2012, 134, 15016−15021.

(6) (a) Nouar, F.; Eubank, J. F.; Bousquet, T.; Wojtas, L.; Zaworotko, M. J.; Eddaoudi, M. J. Am. Chem. Soc. 2008, 130, 1833−1835. (b) Yan, Y.; Lin, X.; Yang, S.; Blake, A. J.; Dailly, A.; Champness, N. R.; Hubberstey, P.; Schröder, M. Chem. Commun. 2009, 1025−1027. (c) Yan, Y.; Telepeni, I.; Yang, S.; Lin, X.; Kockelmann, W.; Dailly, A.; Blake, A. J.; Lewis, W.; Walker, G. S.; Allan, D. R.; Barnett, S. A.; Champness, N. R.; Schröder, M. J. Am. Chem. Soc. 2010, 132, 4092−4094. (d) Yan, Y.; Blake, A. J.; Lewis, W.; Barnett, S. A.; Dailly, A.; Champness, N. R.; Schröder, M. Chem. - Eur. J. 2011, 17, 11162−11170. (e) Yan, Y.; Yang, S.; Blake, A. J.; Lewis, W.; Poirier, E.; Barnett, S. A.; Champness, N. R.; Schröder, M. Chem. Commun. 2011, 47, 9995−9997. (f) Yan, Y.; Suyetin, M.; Bichoutskaia, E.; Blake, A. J.; Allan, D. R.; Barnett, S. A.; Schröder, M. Chem. Sci. 2013, 4, 1731−1736.

(7) (a) Zhang, M.; Chen, Y.-P.; Bosch, M.; Gentle, T., III; Wang, K.; Feng, D.; Wang, Z. U.; Zhou, H.-C. Angew. Chem., Int. Ed. 2014, 53,

815−818. (b) Dincă, M.; Dailly, A.; Long, J. R. *Chem. - Eur. J.* **2008**, *14*, 10280−10285.

(8) (a) Ma, S.; Sun, D.; Ambrogio, M.; Fillinger, J. A.; Parkin, S.; Zhou, H.-C. *J. Am. Chem. Soc.* **2007**, *129*, 1858−1859. (b) Furukawa, H.; Go, Y. B.; Ko, N.; Park, Y. K.; Uribe-Romo, F. J.; Kim, J.; O'Keeffe, M.; Yaghi, O. M. *Inorg. Chem.* **2011**, *50*, 9147−9152.

(9) (a) Oisaki, K.; Li, Q.; Furukawa, H.; Czaja, A. U.; Yaghi, O. M. *J. Am. Chem. Soc.* **2010**, *132*, 9262−9264. (b) Farha, O. K.; Malliakas, C. D.; Kanatzidis, M. G.; Hupp, J. T. *J. Am. Chem. Soc.* **2010**, *132*, 950−952.

(10) Grunder, S.; Valente, C.; Whalley, A. C.; Sampath, S.; Portmann, J.; Botros, Y. Y.; Stoddart, J. F. *Chem. - Eur. J.* **2012**, *18*, 15632−15649.

(11) Deng, H.; Grunder, S.; Cordova, K. E.; Valente, C.; Furukawa, H.; Hmadeh, M.; Gándara, F.; Whalley, A. C.; Liu, Z.; Asahina, S.; Kazumori, H.; O'Keeffe, M.; Terasaki, O.; Stoddart, J. F.; Yaghi, O. M. *Science* **2012**, *336*, 1018−1023.

(12) Lörtscher, E.; Elbing, M.; Tschudy, M.; von Hänisch, C.; Weber, H. B.; Mayor, M.; Riel, H. *ChemPhysChem* **2008**, *9*, 2252−2258.

(13) (a) Reid, C. R.; Thomas, K. M. *Langmuir* **1999**, *15*, 3206−3218. (b) Reid, C. R.; Thomas, K. M. *J. Phys. Chem. B* **2001**, *105*, 10619−10629.

(14) (a) Sheldrick, G. M. *SHELXL2013: Program for Refinement of Crystal Structures*; University of Göttingen: Göttingen, Germany, 2013. (b) Sheldrick, G. M. *Acta Crystallogr., Sect. A: Found. Crystallogr.* **2008**, *64*, 112−122.

(15) Spek, A. L. *Acta Crystallogr., Sect. C* **2015**, *71*, 9−18.

(16) (a) Ortiz, A. U.; Boutin, A.; Fuchs, A. H.; Coudert, F.-X. *J. Chem. Phys.* **2013**, *138*, 174703. (b) Ortiz, A. U.; Boutin, A.; Fuchs, A. H.; Coudert, F.-X. *Phys. Rev. Lett.* **2012**, *109*, 195502.

(17) Tan, J.-C.; Civalleri, B.; Lin, C.-C.; Valenzano, L.; Galvelis, R.; Chen, P.-F.; Bennett, T. D.; Mellot-Draznieks, C.; Zicovich-Wilson, C. M.; Cheetham, A. K. *Phys. Rev. Lett.* **2012**, *108*, 095502.

(18) Ogborn, J. M.; Collings, I. E.; Moggach, S. A.; Thompson, A. L.; Goodwin, A. L. *Chem. Sci.* **2012**, *3*, 3011−3017.

(19) Bouëssel du Bourg, L.; Ortiz, A. U.; Boutin, A.; Coudert, F.-X. *APL Mater.* **2014**, *2*, 124110.

(20) Yan, Y.; Yang, S.; Blake, A. J.; Schröder, M. *Acc. Chem. Res.* **2014**, *47*, 296−307.

(21) (a) Dincă, M.; Long, J. R. *Angew. Chem., Int. Ed.* **2008**, *47*, 6766−6779. (b) Peterson, V. K.; Liu, Y.; Brown, C. M.; Kepert, C. J. *J. Am. Chem. Soc.* **2006**, *128*, 15578−15579.

(22) Rowsell, J. L. C.; Millward, A. R.; Park, K. S.; Yaghi, O. M. *J. Am. Chem. Soc.* **2004**, *126*, 5666−5667.

(23) (a) Peng, Y.; Krungleviciute, V.; Eryazici, I.; Hupp, J. T.; Farha, O. K.; Yildirim, T. *J. Am. Chem. Soc.* **2013**, *135*, 11887−11894. (b) He, Y.; Zhou, W.; Yildirim, T.; Chen, B. *Energy Environ. Sci.* **2013**, *6*, 2735−2744.

(24) Farha, O. K.; Wilmer, C. E.; Eryazici, I.; Hauser, B. G.; Parilla, P. A.; O'Neill, K.; Sarjeant, A. A.; Nguyen, S. B. T.; Snurr, R. Q.; Hupp, J. T. *J. Am. Chem. Soc.* **2012**, *134*, 9860−9863.

(25) Alsmail, N. H.; Suyetin, M.; Yan, Y.; Cabot, R.; Krap, C. P.; Lü, J.; Easun, T. L.; Bichoutskaia, E.; Lewis, W.; Blake, A. J.; Schröder, M. *Chem. - Eur. J.* **2014**, *20*, 7317−7324.

(26) (a) Banerjee, R.; Furukawa, H.; Britt, D.; Knobler, C.; O'Keefe, M.; Yaghi, O. M. *J. Am. Chem. Soc.* **2009**, *131*, 3875−3877. (b) Morris, W.; Leung, B.; Furukawa, H.; Yaghi, O. K.; He, N.; Hayashi, H.; Houndonougbo, Y.; Asta, M.; Laird, B. B.; Yaghi, O. M. *J. Am. Chem. Soc.* **2010**, *132*, 11006−11008.

(27) Eldridge, R. B. *Ind. Eng. Chem. Res.* **1993**, *32*, 2208−2212.

(28) (a) Wu, H.; Gong, Q.; Olson, D. H.; Li, J. *Chem. Rev.* **2012**, *112*, 836−868. (b) He, Y.; Zhou, W.; Krishna, R.; Chen, B. *Chem. Commun.* **2012**, *48*, 11813−11831.

(29) (a) Bloch, E. D.; Queen, W. L.; Krishna, R.; Zadrozny, J. M.; Brown, C. M.; Long, J. R. *Science* **2012**, *335*, 1606−1610. (b) Herm, Z. R.; Bloch, E. D.; Long, J. R. *Chem. Mater.* **2014**, *26*, 323−338. (c) Das, M. C.; Xu, H.; Xiang, S.; Zhang, Z.; Arman, H. D.; Qian, G.; Chen, B. *Chem. - Eur. J.* **2011**, *17*, 7817−7822. (d) Xiang, S. C.; Zhang, Z. J.; Zhao, C. G.; Hong, K.; Zhao, X. B.; Ding, D. R.; Xie, M. H.; Wu, C.

D.; Das, M. C.; Gill, R.; Thomas, K. M.; Chen, B. *Nat. Commun.* **2011**, *2*, 204−209.

(30) Matsuda, R.; Kitaura, R.; Kitagawa, S.; Kubota, Y.; Belosludov, R. V.; Kobayashi, T. C.; Sakamoto, H.; Chiba, T.; Takata, M.; Kawazoe, Y.; Mita, Y. *Nature* **2005**, *436*, 238−241.

(31) (a) Xiang, S.; Zhou, W.; Gallegos, J. M.; Liu, Y.; Chen, B. *J. Am. Chem. Soc.* **2009**, *131*, 12415−12419. (b) He, Y.; Krishna, R.; Chen, B. *Energy Environ. Sci.* **2012**, *5*, 9107−9120.

(32) Xiang, S.; Zhou, W.; Zhang, Z.; Green, M. A.; Liu, Y.; Chen, B. *Angew. Chem., Int. Ed.* **2010**, *49*, 4615−4618.

(33) He, Y.; Zhang, Z.; Xiang, S.; Wu, H.; Fronczek, F. R.; Zhou, W.; Krishna, R.; O'Keeffe, M.; Chen, B. *Chem. - Eur. J.* **2012**, *18*, 1901−1904.